

# Association-mediated chromism of amphiphilic triphenyl-6-oxoverdazyl†

Kentaro Suzuki,<sup>ab</sup> Michio M. Matsushita,<sup>b</sup> Hiroyuki Hayashi,<sup>c</sup> Noboru Koga<sup>c</sup>  
and Tadashi Sugawara<sup>\*ab</sup>

Received (in Montpellier, France) 2nd July 2008, Accepted 11th August 2008

First published as an Advance Article on the web 20th September 2008

DOI: 10.1039/b811207j

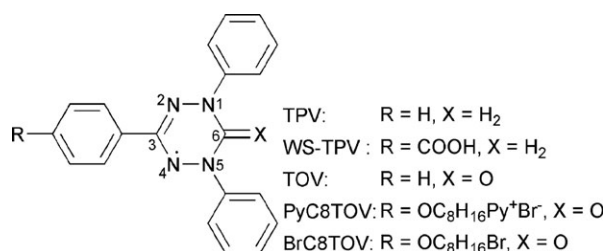
We synthesized a novel amphiphilic compound, 1,5-diphenyl-3-(4-(8-(pyridin-1-ium-1-yl)-octoxy)phenyl)-6-oxoverdazyl bromide (PyC8TOV) thorough modification of 1,3,5-triphenyl-6-oxoverdazyl by introducing a pyridinium head group. This amphiphilic radical dissolved in water at concentrations lower than 0.1 mM but formed aggregates at higher concentrations. Depending on its concentration in water, PyC8TOV afforded crystals, or gels. The solvent- and concentration-dependences of UV and ESR spectra of PyC8TOV are discussed in terms of the environmentally sensitive electronic structure of this amphiphilic radical. The nonlinear dependence of the relaxivity of an aqueous solution of PyC8TOV strongly suggests the formation of aggregates in concentrated solution. PyC8TOV exhibited not only solvatochromism but also association-mediated chromism.

## Introduction

Considerable interest has been focused recently on molecular self-assemblies constructed by amphiphilic molecules in water, such as micelles, bimolecular membranes and vesicles.<sup>1</sup> Many investigations of such self-assemblies have been concerned with local phase separation among multiple amphiphiles in the assembly, with the elasticity of the self-assembly as a whole.<sup>2</sup> To detect such subtle changes in the local environment of these self-assemblies by spectroscopic means, use of water-soluble amphiphilic spin-probes is a powerful, and non-invasive technique.<sup>3</sup> Amphiphilic radicals employed in this manner are useful for biological and medical applications.<sup>4–7</sup> For example, nitroxides are often used as spin-probes to detect local concentrations of superoxides at the surface or within the membrane of blood vessels.<sup>5</sup> These spin-probes can also be used as contrast media in ESRI (ESR imaging; e.g. PEDRI/OMNI)<sup>6</sup> or MRI measurements.<sup>4,7</sup>

We have prepared a novel amphiphilic radical based on 1,3,5-triphenylverdazyl (TPV) to be explored as a spin-probe for the above purpose. Although TPV is a well-known persistent radical<sup>8–13</sup> and has been studied in respect of its magnetic properties<sup>11,12</sup> and reactivities,<sup>13</sup> its behavior in water has scarcely been explored yet. Since the hydrophobicity of TPV is much higher than that of nitroxides (the saturation

concentration of TPV in water is *ca.* 10<sup>−5</sup> M),<sup>14</sup> amphiphilic TPV must be more firmly held by membranes. Mayr *et al.* reported the pioneering synthesis of the water-soluble TPV (WS-TPV) radical.<sup>15</sup> However, the hydrophilic moiety of this radical is a carboxylic group that permits the WS-TPV to dissolve only in alkaline water (pH > 10). Furthermore, the concentration dependence of UV and ESR spectra for WS-TPV is small.



The novel amphiphilic TPV-based radical discussed in this paper is endowed with two chemical modifications. First, a long alkyl chain bearing a pyridinium ion at the end is introduced to increase its solubility and self-aggregation ability in water over a wide pH range.<sup>1,2</sup> Second, a 1,3,5-triphenyl-6-oxoverdazyl (TOV) unit, which is a carboxo-derivative of TPV, is used *in lieu* of TPV to contact with water locally as a radical unit. When the methylene group at the 6-position of TPV is replaced with a carboxo group to form TOV, the spin-densities of TOV become inequivalent.<sup>9,10</sup> Accordingly, the electronic structure of TOV becomes sensitive to the presence of water due to the contribution of its zwitterionic form (Scheme 1).

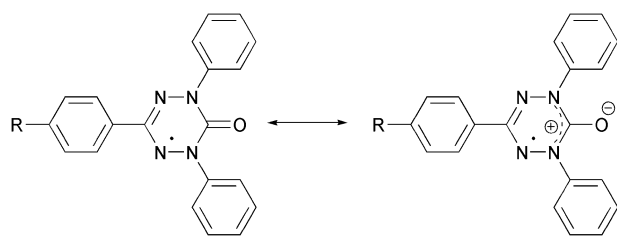
We found that our novel amphiphilic TOV, 1,5-diphenyl-3-(4-(8-(pyridin-1-ium-1-yl)octoxy)phenyl)-6-oxoverdazyl bromide (PyC8TOV; Py = pyridyl bromide), dissolves in water and forms a self-aggregate, a glue or crystals, depending on the concentration of PyC8TOV in aqueous solution. Notably,

<sup>a</sup> Department of Basic Science, Graduate School of Arts and Sciences, The University of Tokyo, 3-8-1 Komaba, Meguro, Tokyo 153-8902, Japan. E-mail: suga@pentacle.c.u-tokyo.ac.jp; Fax: +81-3-5454-6997; Tel: +81-3-5454-6742

<sup>b</sup> Research Centre for Life System as Complex Systems, Department of Basic Science, Graduate School of Arts and Sciences, The University of Tokyo, 3-8-1 Komaba, Meguro, Tokyo 153-8902, Japan

<sup>c</sup> Department of Chemo-Pharmaceutical Sciences, Graduate School of Pharmaceutical Science, Kyushu University, 3-1-1 Maidashi, Higashi, Fukuoka 812-8582, Japan

† CCDC reference number 698233. For crystallographic data in CIF or other electronic format see DOI: 10.1039/b811207j



Scheme 1

these forms of PyC8TOV exhibit not only solvatochromism but also association-mediated chromism in aqueous solution, presumably due to the high hydrophobicity of TOV and the specific interaction between its carboxo-group and the surrounding polar protic solvents.

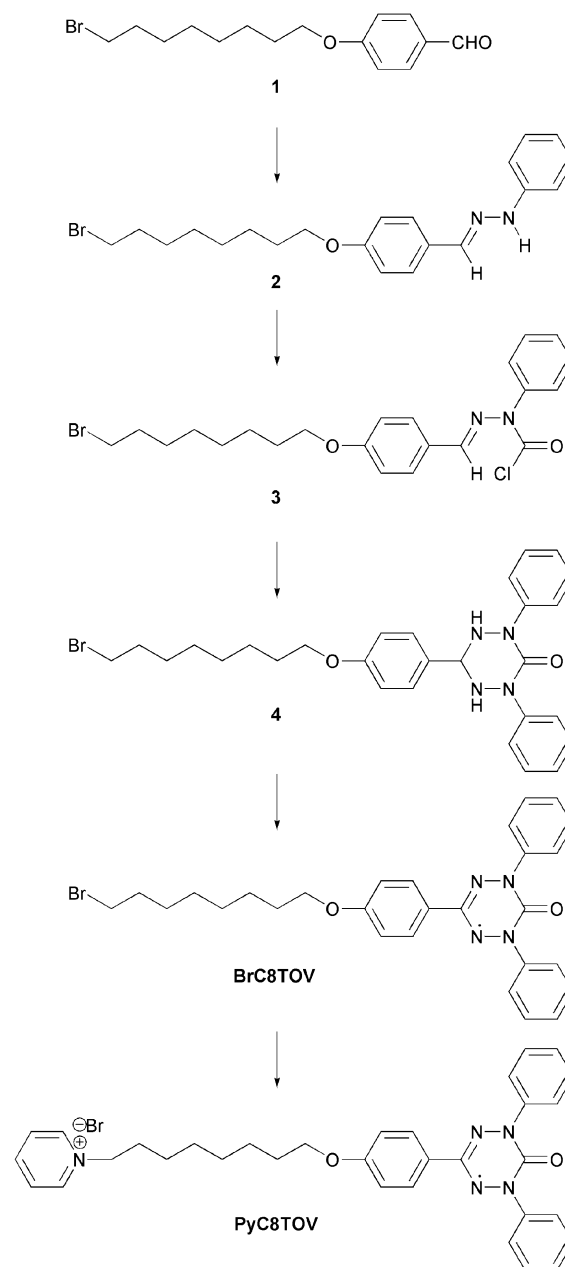
## Experimental

### Measurements

UV-Vis spectra of organic and aqueous solutions of PyC8TOV at ambient temperature were measured with a Shimadzu UV-3150 UV-Vis-NIR Spectrophotometer. X-Band ESR spectra of a polycrystalline sample of PyC8TOV, a chloroform and an de-ionized water solution of PyC8TOV and a benzene solution of BrC8TOV were recorded on a JEOL JES-TE300 ESR spectrometer. The concentration dependence of the  $T_1$ -relaxation time of PyC8TOV in aqueous solution at 25 °C was measured with a JEOL JNM-MU25A pulse NMR spectrometer. The particle size distribution of PyC8TOV micellar aggregates in aqueous solution was measured by means of dynamic light scattering in the range of 0.01–5  $\mu\text{m}$  with a Nikkiso Microtrac IPA-150 particle-size distribution analyzer. Microscopic images were observed under an Olympus IX71 phase contrast/fluorescence microscope equipped with a Hamamatsu Photonics ORCA-ER cooled CCD camera. Cryogenic scanning electron microscopy (Cryo-SEM) images were obtained with a Hitachi S3000N scanning electron microscope operating at liquid-nitrogen temperature. The temperature dependence of the magnetic susceptibility of a glue-like sample of PyC8TOV, polycrystals of BrC8TOV and PyC8TOV $\cdot$ 1.5H $_2$ O were measured individually with a Quantum Design MPMS-5 SQUID magnetometer in a temperature range of 2–300 K, the applied magnetic field being 0.5 T. The susceptibility data were corrected by subtracting the diamagnetic component evaluated by extrapolating the magnetic data at higher temperatures.

### Synthesis of PyC8TOV

The amphiphilic TOV radical 1,5-diphenyl-3-(4-(8-(pyridin-1-ium-1-yl)octoxy)phenyl)-6-oxoverdazyl bromide (PyC8TOV) was synthesized by modifying the procedure reported by Neugebauer *et al.*<sup>10</sup> (Scheme 2). Chemicals were obtained from commercial sources and used without further purification. Phenyl hydrazine (3.8 mg, 35 mmol) was added to a suspension of 4-(8-bromooctoxy)benzaldehyde (12 g,



**Scheme 2** Reagents and conditions: (i) phenylhydrazine; (ii) triphosgene, pyridine; (iii) phenylhydrazine, triethylamine; (iv) silver(I) oxide; (v) pyridine.

38 mmol; **1**) in ethanol–toluene (1 : 1 v/v), which was prepared according to the literature procedure,<sup>16</sup> and the mixture was refluxed for 2 h. After cooling to room temperature, the precipitated product was filtered and dried *in vacuo* to afford 4-(8-bromooctoxy)benzaldehyde phenylhydrazone, **2**, as a white powder (11 g, 70% yield). Under a nitrogen atmosphere, **2** (10 g, 2.4 mmol) and anhydrous pyridine (2.3 g, 29 mmol) were dissolved in anhydrous toluene (200 mL), and the mixture was cooled to 5 °C. A solution of triphosgene (2.8 g, 8.0 mmol) in anhydrous toluene (50 mL) was added dropwise to the cooled solution, and the mixture was refluxed for 2 h. The resulting mixture was filtered through a short silica gel column to remove pyridine hydrochloride salt, and the filtrate

was evaporated. The crude product, 4-(8-bromooctoxy)-benzaldehyde 2-chloroformyl-2-phenylhydrazone (**3**), was dissolved in chloroform; phenylhydrazine (2.2 g, 20 mmol) and triethylamine (2.2 g, 22 mmol) were added to this solution; and the mixture was stirred for 12 h at room temperature. The reaction mixture was washed with water followed by saturated aqueous  $\text{NaHCO}_3$  (for removing triethylamine hydrochloride salt), dried by sodium sulfate and evaporated. The crude product was purified by recrystallization from dichloromethane-methanol to afford 1,4,5,6-tetrahydro-2,4-diphenyl-6-(4-(8-bromooctoxyphenyl))-1,2,4,5-tetrazine-3(2*H*)-one, **4** (6 g, 38% yield) as a colorless powder. To a solution of **4** (1 g, 1.9 mmol) in 10 mL dichloromethane was added  $\text{Ag}_2\text{O}$  (3 eq.), and the mixture was stirred for 1 h at room temperature. After filtration to remove excess  $\text{Ag}_2\text{O}$ , the resulting solution was purified by silica-gel column chromatography using  $\text{CH}_2\text{Cl}_2$  as the eluent, and the product was recrystallized in ethanol to afford 1,5-diphenyl-3-(4-(8-bromooctoxy)phenyl)-6-oxoverdazyl (BrC8TOV) as a dark green powder (640 mg, 64% yield); mp 81–83 °C (from ethanol); ESR (benzene):  $g = 2.0032$ ,  $a/m\text{T}$  0.651 ( $\text{N}_{1,5}$ ), 0.448 ( $\text{N}_{2,4}$ ). A 50-mL solution of anhydrous pyridine containing BrC8TOV (400 mg, 0.74 mmol) was refluxed for 30 h to afford PyC8TOV as a dark blue, deliquescent glue-like compound (450 mg, quant.). The glue-like product was recrystallized from water at 40 °C to afford  $\text{PyC8TOV} \cdot 1.5\text{H}_2\text{O}$  as dark green, needle-like crystals; mp 133 °C (decomp., from water);  $\lambda_{\text{max}}(\text{CHCl}_3)/\text{nm}$ : 269 ( $\epsilon/\text{dm}^3 \text{ mol}^{-1} \text{ cm}^{-1}$ : 25 200), 274 (25 300), 313 (11 900, sh), 330 (10 300, sh) 577 (1700);  $m/z$  (MALDI-TOF): 534.3 ( $\text{M}^+ + \text{H} - \text{Br}$ .  $\text{C}_{33}\text{H}_{36}\text{N}_5\text{O}_2$  requires 534.29); ESR ( $\text{CHCl}_3$ ):  $g = 2.0033$ ,  $a/m\text{T}$  0.65 ( $\text{N}_{1,5}$ ), 0.45 ( $\text{N}_{2,4}$ ). Purities of BrC8TOV and PyC8TOV were evaluated by determining their magnetic susceptibilities (*vide infra*).

#### X-Ray crystal structural analysis of $\text{PyC8TOV} \cdot 1.5\text{H}_2\text{O}$

X-Ray crystallographic analysis of a single crystal of  $\text{PyC8TOV} \cdot 1.5\text{H}_2\text{O}$  was carried out at room temperature with a Rigaku Mercury CCD X-ray diffractometer with graphite-monochromatized Mo- $\text{K}\alpha$  radiation ( $\lambda = 0.71073 \text{ \AA}$ ; 50 kV, 250 mA). The crystal, sized  $0.50 \times 0.10 \times 0.02 \text{ mm}$ , was fixed at the top of a thin glass capillary by Araldite glue. The structure was solved by direct method (SHELXS-97) and refined by full-matrix least squares (SHELXL-97).<sup>17</sup> Hydrogen atoms were introduced at calculated positions (riding method). The asymmetric unit contains two PyC8TOV and three  $\text{H}_2\text{O}$  molecules. One molecule shows disorder at the octamethylene unit while the other conformer does not. The ratio of the major and minor set of the disorder were optimized to be 0.64 : 0.36 upon refinement.

**Crystallographic data for  $\text{PyC8TOV} \cdot 1.5\text{H}_2\text{O}$ .** Black plate, size  $0.50 \times 0.10 \times 0.02 \text{ mm}$ ,  $\text{C}_{33}\text{H}_{38}\text{BrN}_5\text{O}_{3.5}$ ,  $M_r = 640.60$ , triclinic, space group  $P\bar{1}$  (no. 2),  $\lambda(\text{Mo-K}\alpha) = 0.71073 \text{ \AA}$ ,  $T = 293(2) \text{ K}$ ,  $a = 10.2900(5)$ ,  $b = 14.210(1)$ ,  $c = 22.722(2) \text{ \AA}$ ,  $\alpha = 78.55(1)$ ,  $\beta = 82.28(1)$ ,  $\gamma = 79.98(1)^\circ$ ,  $V = 3189.4(4) \text{ \AA}^3$ ,  $Z = 4$ ,  $D_c = 1.334 \text{ g cm}^{-3}$ . Isotropic and anisotropic least-squares refinement (763 parameters) on 13831 merged

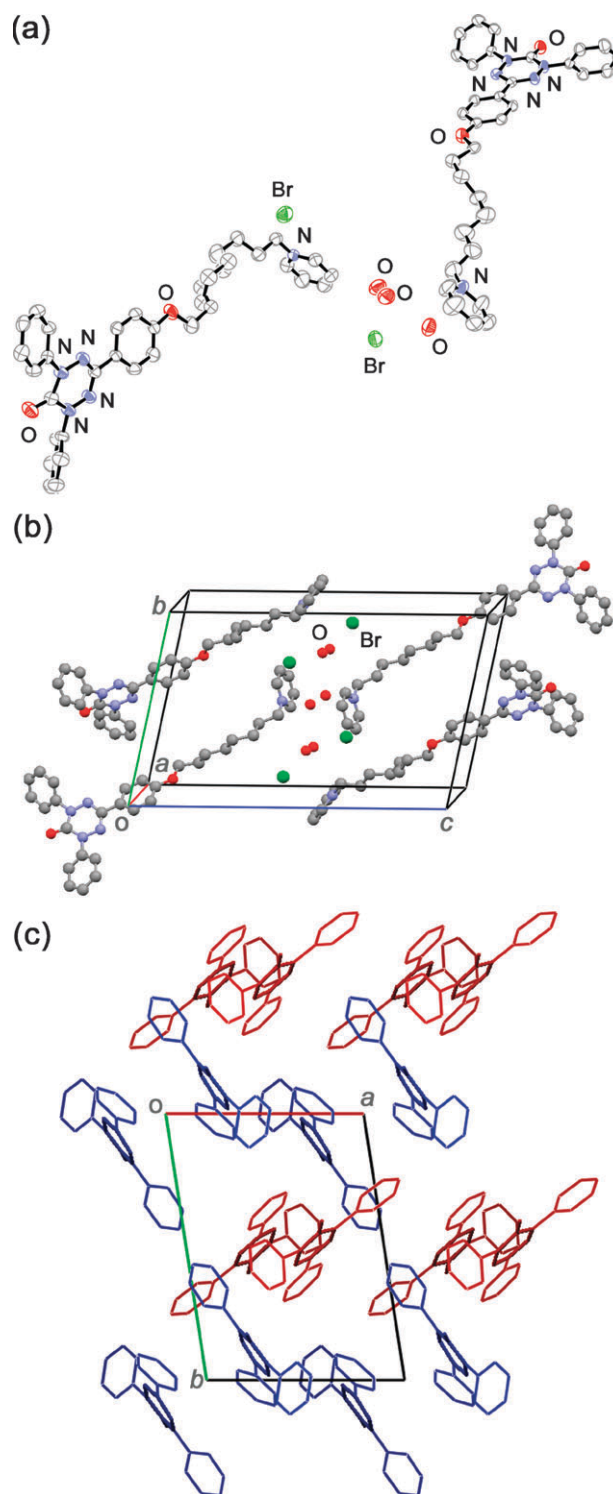


**Fig. 1** Crystal structure of  $\text{PyC8TOV} \cdot 1.5\text{H}_2\text{O}$ .<sup>17</sup> (a) ORTEP drawing (50% probability chosen for the ellipsoids). (b) Crystal structure, viewed along the  $a^*$ -axis. (c) Stacking of the two kinds of crystallographically independent PyC8TOV molecules (red and blue). For clarity, only the triphenyl-6-oxoverdazyl part is shown.

reflections ( $R_{\text{int}} = 0.0464$ ) converged at  $R_{\text{all}} = 0.1703$  for all data;  $R_I > 2\sigma(I) = 0.0623$  for 5970 observed data ( $I > 2\sigma(I)$ ), GOF = 0.960.

## Results and discussion

### Crystal structure of PyC8TOV

Each asymmetric unit contains two crystallographically independent radical molecules, two bromide ions and three water molecules (Fig. 1(a)). Two crystallographically independent radicals are observed, which differ in the conformation of their alkyl chains and in the dihedral angles of their aromatic planes. Crystal water molecules are located around the pyridinium ion site, not at the radical site, forming a hydrogen-bonded cluster with counter-anions located between the layers of radical molecules; PyC8TOV does not interact with these hydrogen-bonded clusters as shown in Fig. 1(b). Thus, the radical molecules and hydrogen-bonded counter-anions form a layered structure along the *c*-axis: these two types of conformers are shown in Fig. 1(c) as red and blue molecules. Each conformer forms head-to-tail dimers with inversion symmetry and the dimers stack along the *a*-axis, forming two distinct columns. One column consists of an almost regular stacking, although the intermolecular distance is rather remote and no  $\pi$ - $\pi$  overlapping is recognized. In contrast, a dimeric structure is observed in the other column. These two types of columns arrange alternately along the *b*-axis to form a sheet-like structure within the *ab* plane (Fig. 1(c)).

### Magnetic properties of PyC8TOV and BrC8TOV

The temperature dependence of the magnetic susceptibilities of microcrystalline PyC8TOV·1.5H<sub>2</sub>O, the glue-like sample of PyC8TOV and microcrystalline BrC8TOV were measured by a SQUID magnetometer (Fig. 2). The purities of all radicals were confirmed by their Curie constants near room temperature. The antiferromagnetic behavior of microcrystalline PyC8TOV·1.5H<sub>2</sub>O (Fig. 2, filled circles) was interpreted in terms of the Curie–Weiss law (Curie constant,

$C = 0.376 \text{ emu K mol}^{-1}$ ; Curie–Weiss temperature,  $\theta = -7.2 \text{ K}$ ). The Curie constant ( $0.376 \text{ emu K mol}^{-1}$ ) of the anhydrous glue-like PyC8TOV (Fig. 2, open circles) was reproduced by 44% of the paramagnetic component ( $\theta \sim 0 \text{ K}$ ) and 56% of the antiferromagnetic component ( $\theta \sim -30 \text{ K}$ ), indicating that the amorphous PyC8TOV sample contained both paramagnetic and the antiferromagnetic domains. This result suggests that the magnetic interaction between the amphiphilic PyC8TOV radicals is negligibly small when they are randomly arranged, whereas approximately half of the radicals form a tight antiferromagnetic stacking. The temperature dependence of the magnetic susceptibility of BrC8TOV (Fig. 2, triangles) was analyzed by the antiferromagnetic dimer model<sup>18</sup> with  $C = 0.375 \text{ emu K mol}^{-1}$ ,  $\theta = -12 \text{ K}$  and an intradimer interaction,  $2J/k_B$ , of  $-37.5 \text{ K}$ .

### Concentration dependence of UV spectra in aqueous solution

PyC8TOV dissolved in de-ionized water or in standard phosphate buffered solutions with pH values of 10.1, 7.41, 6.86 or 4.01. Though a  $<1 \text{ mM}$  aqueous solution of PyC8TOV was red (absorption maximum of verdazyl radical,  $\lambda_{\text{max}} = 540 \text{ nm}$ ), solutions more concentrated than  $1 \text{ mM}$  exhibited a blue color ( $\lambda_{\text{max}} = 575 \text{ nm}$ ), as shown by the absorption spectra in Fig. 3(a). The critical concentration for this observed color change was estimated to be  $0.1 \text{ mM}$  by extrapolating the concentration dependence of  $\lambda_{\text{max}}$  as shown in Fig. 3(b). Namely, the absorption maximum remained at  $540 \text{ nm}$  (red) at concentrations lower than  $0.1 \text{ mM}$  and red-shifted linearly to  $586 \text{ nm}$  (blue) as the concentration increased, though the absorption coefficient,  $\epsilon$ , was maintained at nearly constant values throughout (Fig. 3(a)). In contrast, a chloroform solution of PyC8TOV showed a blue color, which was similar to the concentrated aqueous solution of PyC8TOV, and the concentration dependence of  $\lambda_{\text{max}}$  was very small.

To evaluate the size distribution of PyC8TOV aggregates, a  $1 \text{ mM}$  aqueous solution of PyC8TOV was sonicated for 20 min and then subjected to dynamic light scattering analysis 6 h after sonication. Although the size distribution of the aggregates was scattered immediately after sonication, it converged within 6 h, with aggregate sizes ranging from  $0.1$  to  $1.2 \mu\text{m}$  and a maximum frequency at *ca.*  $0.2 \mu\text{m}$  (Fig. 4). Moreover, a concentrated ( $>20 \text{ mM}$ ) aqueous solution of PyC8TOV formed a gel (Fig. 5(a) with an inverse hexagonal (H<sub>II</sub>) phase) structure,<sup>19</sup> containing *ca.*  $5 \mu\text{m}$  channels as shown by Cryo-SEM (Fig. 5(b)). The melting point of this gel was *ca.*  $45 \text{ }^\circ\text{C}$ , and the gel crystallized upon prolonged standing.

Furthermore, a red aqueous solution of PyC8TOV ( $0.25 \text{ mM}$ ) turned blue upon the addition of  $>10 \text{ mM}$  sodium chloride (Fig. 6). This color change was likely due to aggregation of PyC8TOV caused by the charge-screening (or “salting-out”) effect<sup>2</sup> of the added sodium chloride. An aqueous solution of PyC8TOV containing  $10$ – $100 \text{ mM}$  sodium chloride exhibited  $\lambda_{\text{max}}$  of *ca.*  $575 \text{ nm}$ , which was almost the same as that observed for the chloroform solution described above. These results indicate that PyC8TOV exhibited association-mediated chromism.

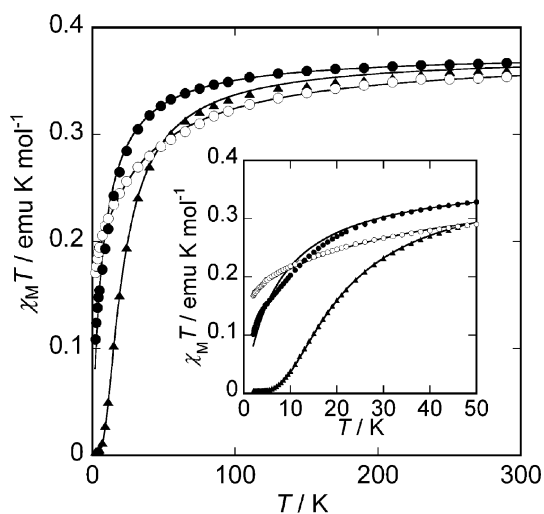


**Fig. 2** Temperature dependence of magnetic susceptibilities of microcrystalline PyC8TOV·1.5H<sub>2</sub>O (●), glue-like, anhydrous PyC8TOV (○) and microcrystalline BrC8TOV (▲) as determined by SQUID magnetometer. The solid lines are theoretical fits corresponding to each magnetic structure (see text). Inset: magnified drawing of the low temperature region.

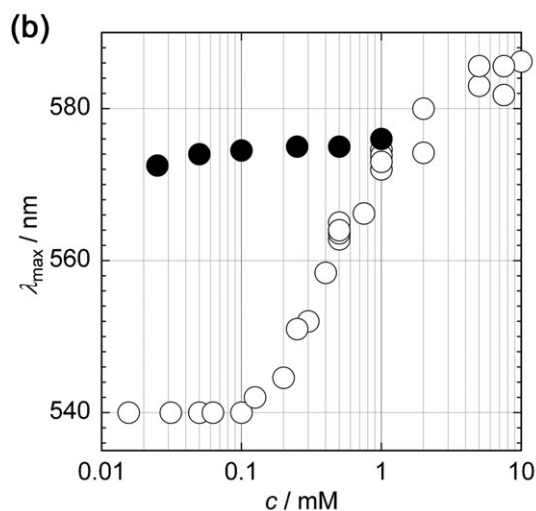
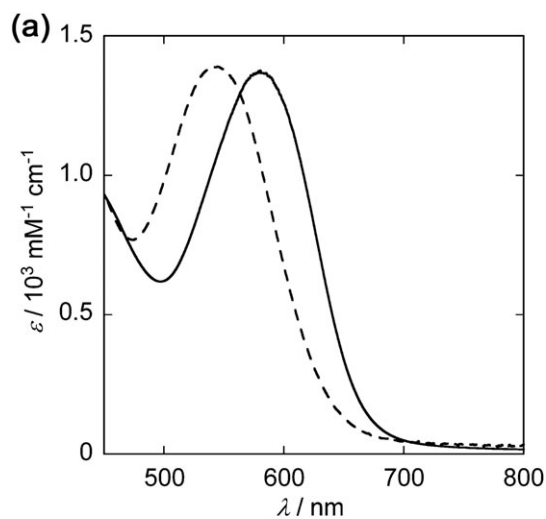


**Fig. 3** (a) UV-Vis spectra of PyC8TOV dissolved in water at concentrations of 2.0 (—) and 0.125 (---) mM. (b) Concentration dependence of  $\lambda_{\max}$  of PyC8TOV dissolved in water (○) and in  $\text{CHCl}_3$  (●).

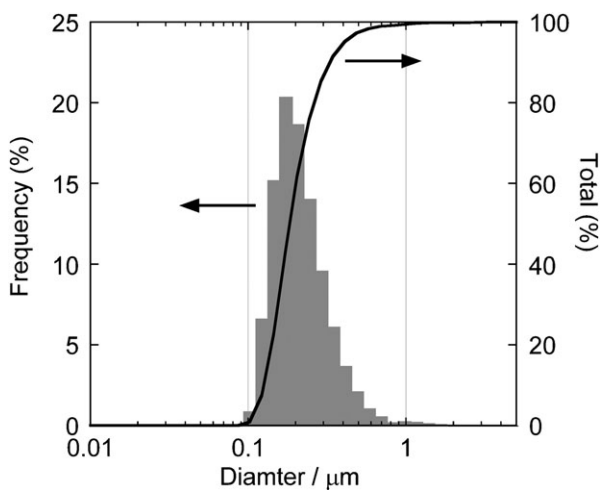


**Fig. 4** PyC8TOV aggregate size distribution measurements obtained by dynamic light scattering analysis of a 1 mM aqueous solution of PyC8TOV.

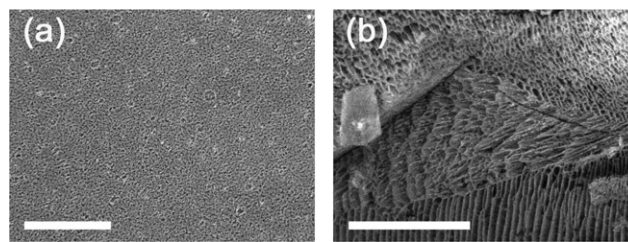


**Fig. 5** Phase contrast microscopic image (a) and cryo-SEM image (b) of a 20 mM aqueous solution of PyC8TOV. Scale bars: 100  $\mu\text{m}$ .



**Fig. 6** Observed color change of a 0.25 mM aqueous solution of PyC8TOV (red, left) caused by the addition of 50 mM NaCl (blue, right).

Bathochromic shifts in absorption spectra caused by the formation of J-aggregates have been well studied.<sup>20</sup> Such shifts are derived from the coupling between transition dipoles of chromophores that interact intensely upon arrangement into an aggregate structure. Additionally, an intense increase in absorbance typically accompanies such bathochromic shifts. However, no enhanced absorbance upon the formation of aggregates was observed in the current experiment (Fig. 3(b)). Accordingly, the concentration dependence of the observed color change cannot be ascribed to the formation of J-aggregates.

#### Concentration dependence of ESR spectra in aqueous solution

ESR spectroscopic measurement of PyC8TOV was performed in aqueous and non-aqueous solutions and it was found that the spectrum in a diluted aqueous solution is different from those measured in other conditions (Table 1 and Fig. 7). The  $g$ -values in a 1.0 mM aqueous solution, in a chloroform solution, and of the polycrystalline  $\text{PyC8TOV} \cdot 1.5\text{H}_2\text{O}$  were *ca.* 2.003. Reference samples (BrC8TOV, TOV and TPV) also showed similar  $g$ -values. On the other hand, the spectrum of a 0.5 mM aqueous solution<sup>21</sup> showed a  $g$ -value of 2.0041, being slightly larger than others.

The hyperfine structure constants (hfsc's) of nitrogen atoms in a verdazyl ring,  $a(\text{N})$ , at the 1,5- and 2,4-positions of 1,3,5-triphenylverdazyl (TPV) are the same as aforementioned;  $a(\text{N}_{1,5}) = 0.6$  mT and  $a(\text{N}_{2,4}) = 0.6$  mT.<sup>9</sup> However, they become inequivalent,  $a(\text{N}_{1,5}) = 0.45$  mT and  $a(\text{N}_{2,4}) = 0.65$  mT, in 1,3,5-triphenyl-6-oxoverdazyl (TOV).<sup>10</sup> The difference between  $a(\text{N}_{1,5})$  and  $a(\text{N}_{2,4})$  values of all TOV derivatives in Table 1 is 0.2 mT. However, the absolute value of  $a(\text{N}_{1,5})$  and  $a(\text{N}_{2,4})$  of PyC8TOV in 0.5 mM aqueous solution were appreciably larger than others. This discrepancy indicates

**Table 1** ESR parameters of a microcrystal, aqueous and non-aqueous solutions of PyC8TOV, and reference verdazyl radicals

Radical	Solvent	$c/\text{mM}$	$a(N_{1,s})/\text{mT}$	$a(N_{1,s})/\text{mT}$	$g$
PyC8TOV	Water	0.5	0.47	0.67	2.0041
	Water	1	n.d. <sup>a</sup>	n.d. <sup>a</sup>	2.0033
	CHCl <sub>3</sub>	0.5, 1	0.448	0.651	2.0033
	Polycrystal		n.d. <sup>a</sup>	n.d. <sup>a</sup>	2.0030
BrC8TOV	Benzene	0.5, 1	0.45	0.65	2.0032
TPV <sup>9</sup>	Benzene		0.6	0.6	2.0033
WS-TPV <sup>15</sup>	Water <sup>b</sup>	1	0.6	0.6	
TOV <sup>10</sup>	Toluene		0.450	0.645	2.0037

<sup>a</sup> Not detected. <sup>b</sup> With 1 mM  $\gamma$ -cyclodextrin.

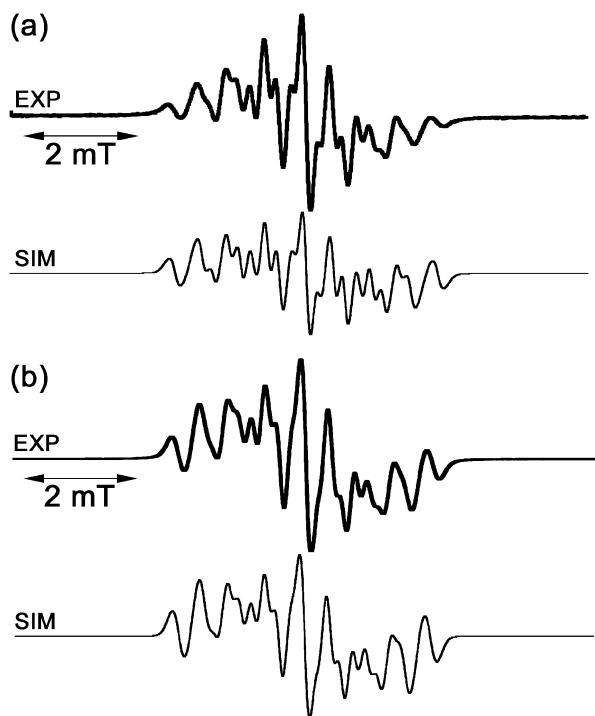


**Fig. 7** ESR spectra and their simulations for 0.5 mM PyC8TOV in water (a) and for 0.5 mM BrC8TOV in benzene (b). The intensities of the central resonance lines for PyC8TOV could not be reproduced accurately by simulation, possibly because of the contribution of the aggregated species in the aqueous solution.

that the larger spin densities reside on four nitrogen atoms of PyC8TOV in a diluted aqueous solution.

Incidentally, the ESR spectrum of a 1 mM aqueous solution of PyC8TOV did not exhibit hfsc, but only a broad signal (peak-to-peak line width,  $\Delta H_{pp}$ ,  $\sim 0.8$  mT) was obtained. This broadening of the resonance lines may be ascribed to the aggregation of PyC8TOV in a concentrated aqueous solution (*vide infra*).

#### $T_1$ relaxation time measurement in aqueous solution

To elucidate the extent of PyC8TOV aggregation in water,  $T_1$  relaxation times of aqueous PyC8TOV solutions were measured by means of the inversion recovery method using pulse <sup>1</sup>H NMR (Fig. 8). The inverse of the longitudinal relaxation time,  $T_1^{-1}$ , increased with increasing concentrations of PyC8TOV in water only at concentrations  $< 0.5$  mM;  $T_1^{-1}$  markedly deviated from this relationship at higher concentrations.

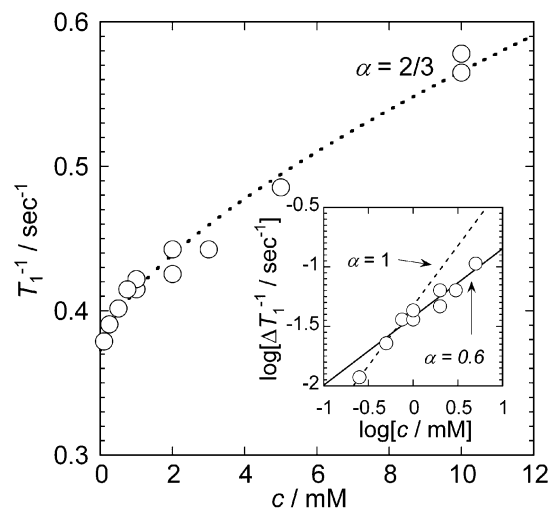


**Fig. 8** Concentration dependence of  $T_1^{-1}$  for an aqueous solution of PyC8TOV. The dashed line corresponds to a two-thirds law fit ( $T_1^{-1} = \gamma c^\alpha + \text{const.}$ ,  $\alpha = 3/2$ ). Inset: log-log plot ( $\Delta T_1^{-1} = T_1^{-1} - T_1^{-1}|_{c=0.25 \text{ mM}}$ ).

Since the gradient of the concentration dependence of  $T_1^{-1}$  is a measure of the relaxivity,  $\gamma$  of the paramagnetic species toward protons in the solvent, the heavy deviation suggests that the interaction between the radical site of the amphiphile and the protons in water was suppressed due to the aggregation of the amphiphilic radicals at high concentration. The correlation between  $T_1^{-1}$  and the concentration of the amphiphilic radicals was linear at concentrations  $< 0.5$ –1 mM, but at higher concentrations in which the aggregates formed ( $> 0.5$ –1 mM), the correlation followed a *ca.* 0.6 ( $\sim 2/3$ ) power law (Fig. 8 inset). Under the assumption that mainly spherical aggregates were generated, these results suggest that the radicals at the surface of the spherical aggregates effectively induced the relaxation of water protons, because the total surface area of a spherical particle is proportional to two-thirds ( $\sim 0.67$ ) of its total volume.

The reason why the critical concentration of aggregate formation estimated by the  $T_1$  relaxation time measurement is larger than that determined by the UV spectral measurement may be explained as follows. Although the aggregates are formed at concentrations higher than 0.1 mM, the size of the aggregates is small and most of the amphiphilic radicals are located at the surface, interacting with water molecules. A deviation from the linear correlation between the  $T_1$  values and the concentration of the amphiphilic radical can not be

observed until the size of the aggregate becomes large enough to have an inner filled structure.

### Association-mediated chromism

The nonlinear change of the concentration dependence of UV and ESR spectra of PyC8TOV occurred at nearly the same concentration ( $\sim 0.1$  mM) as the critical concentration for aggregate formation. Accordingly, the color change observed in an aqueous solution of PyC8TOV indicated the formation of aggregates.

The inverse of absorption maxima ( $\lambda_{\max}^{-1}$ ) of a solution of amphiphilic radicals is proportional to the HOMO–LUMO energy gap ( $\Delta E$ ) of the solvent molecule, and  $\Delta E (\propto \lambda_{\max}^{-1})$  changes sensitively with changes in the polarity of the solvent.<sup>22</sup> When  $\lambda_{\max}^{-1}$  of PyC8TOV in polar protic solutions were plotted against the permittivity ( $\epsilon_p$ ) of the solvents (C–F, without A and B), a steep linear dependence was observed as shown in Table 2 and Fig. 9. Additionally, the  $\lambda_{\max}^{-1}$  value in water ( $\epsilon_p = 80$ ) adhered to this linear dependence at concentrations lower than 0.1 mM (Fig. 9, point A). If  $\lambda_{\max}^{-1}$  of a concentrated aqueous solution ( $> 2$  mM) of PyC8TOV is also plotted in Fig. 9 as point B, assuming  $\epsilon_p = 80$ , it is located far down from the straight line. The extremely small  $\lambda_{\max}^{-1}$  suggests that the effective  $\epsilon_p$  of the sample in the concentrated aqueous solution must be very small. Plots of polar aprotic solvents (points G–K), except acetonitrile (I), are also fitted with a straight line, although its slope is much more gradual: the upward deviation of I (acetonitrile) suggests a specific interaction with PyC8TOV.<sup>23</sup> In nonpolar solvents, such as chloroform (L) and dichloromethane (M), the values of  $\lambda_{\max}^{-1}$  remain almost constant, regardless both of the permittivity and of the concentration.

Although a similar tendency is observed for WS-TPV,<sup>15</sup> the difference in  $\lambda_{\max}^{-1}$  of TPV between the dispersed state and the aggregated state is one-fourth of the corresponding difference for PyC8TOV (points A and B). This observation indicates that the slope of  $\lambda_{\max}^{-1}$  vs. permittivity for WS-TPV might be much smaller than that of PyC8TOV. This observation also strongly suggests that the steep slope observed for PyC8TOV in polar protic solvents can be ascribed partly to the specific hydrogen-bond-type interactions between the

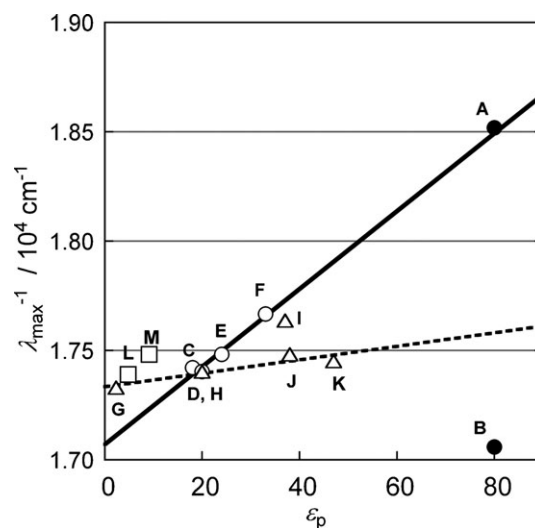


**Fig. 9** Variation of  $\lambda_{\max}^{-1}$  of PyC8TOV in aqueous solutions (A:  $c < 0.1$  mM, B:  $c > 2$  mM), isopropanol (C), *n*-propanol (D), ethanol (E), methanol (F), 1,4-dioxane (G), acetone (H), MeCN (I), DMF (J), DMSO (K),  $\text{CHCl}_3$  (L),  $\text{CH}_2\text{Cl}_2$  (M). The solid and dashed lines are obtained by a least-square method for protic polar solvents (C–F), and aprotic polar ones (G–H, J and K), excepting MeCN,<sup>23</sup> respectively.

carboxo group at the 6-position of PyC8TOV and the protic solvent. As clearly shown by the crystal structure of the hydrated crystal of *p*-acetamidophenyl-2,4-dimethyl-6-oxoverdazyl, the 6-carboxo group is hydrogen-bonded with water molecules in the crystal.<sup>24</sup>

### Conclusion

A novel amphiphilic radical, PyC8TOV, exhibited not only solvatochromism but also association-mediated chromism. The solvent and concentration dependences of UV and ESR spectra of PyC8TOV are explained in terms of the environmentally sensitive electronic structure of this amphiphilic radical. Namely, red solutions of dispersed radicals in water changed to blue solutions of aggregated radicals as the PyC8TOV concentration was increased. The nonlinear dependence of the relaxivity of PyC8TOV was consistent with the above

**Table 2** UV spectroscopic data of solutions of PyC8TOV and WS-TPV<sup>15</sup> in several solvents

Radical	Solvent	Polarity	$\epsilon_p$	$c/\text{mM}$	$\lambda_{\max}/\text{nm}$	$\lambda_{\max}^{-1}/\text{cm}^{-1}$	Color	Symbol <sup>a</sup>
PyC8TOV	Water	Polar (protic)	80	$< 0.1$	540 <sup>b</sup>	18 500	Red	A
	Water	Polar (protic)	80	$> 2$	586 <sup>b</sup>	17 100	Blue	B
	IPA	Polar (protic)	18	0.5	574	17 400	Purple	C
	NPA	Polar (protic)	20	0.5	575	17 400	Purple	D
	EtOH	Polar (protic)	24	0.5	572	17 500	Purple	E
	MeOH	Polar (protic)	33	0.5	566	17 700	Purple	F
	1,4-Dioxane	Polar (aprotic)	2.3	0.5	577	17 300	Purple	G
	Acetone	Polar (aprotic)	20	0.5	575	17 400	Purple	H
	MeCN <sup>23</sup>	Polar (aprotic)	37	0.5	564	17 700	Purple	I
	DMF	Polar (aprotic)	38	0.5	572	17 500	Purple	J
	DMSO	Polar (aprotic)	47	0.5	573	17 500	Purple	K
	$\text{CHCl}_3$	Non-polar	4.8	0.05–1	572–576 <sup>b</sup>	17 400–17 500	Purple	L
	DCM	Non-polar	9.1	0.5	572	17 500	Purple	M
	WS-TPV	Water	Polar (protic)	80	$< 0.1$	706	14 200	Green
Water		Polar (protic)	80	<i>ca.</i> 10	727	13 800	Green	

<sup>a</sup> See Fig. 9. <sup>b</sup> See Fig. 3.

observations. The steeply linear correlation between the  $\lambda_{\max}$  values and the permittivities of PyC8TOV in polar protic solvents suggests that the carboxo group at the 6-position of the verdazyl group specifically interacts with water (or polar protic solvents), reflecting the contribution of the zwitterionic structure (Scheme 1). Since PyC8TOV was soluble in water in a wide pH range, it may be used in various media, including biological systems, as a spin-probe for some specific purposes.

## Acknowledgements

This work was partly supported by KAKENHI (Grant-in-Aid for Scientific Research) on Priority Areas "Application of Molecular Spins" (Area No. 769, Proposal No. 15087101) and on Priority Area "Soft Matter Physics" (Area No. 463).

## References

- (a) M.-A. Guedeau-Boudeville, A.-L. Bernard, J.-C. Bradley, A. Singh and L. Jullien, in *Giant Vesicles*, eds. P.-L. Luisi and P. Walde, John Wiley & Sons, New York, 2000, ch. 26, pp. 341–349; (b) K. Velonia, J. J. L. M. Cornelissen, M. C. Feiters, A. E. Rowan and R. J. M. Nolte, in *Nanoscale Assembly: Chemical Techniques*, ed. W. T. S. Huck, Springer Science + Business Media, New York, 2005, ch. 7, pp. 119–185; (c) T. Kunitake, *Angew. Chem., Int. Ed. Engl.*, 1992, **39**, 709–726.
- (a) C. Taupin, in *Soft Matter Physics*, eds. M. Daoud and C. E. Williams, Springer, Berlin, 1999, ch. 4, pp. 133–150; (b) I. W. Hamley, *Introduction to Soft Matter—Polymers, Colloids, Amphiphiles and Liquid Crystals*, John Wiley & Sons, New York, 2000.
- (a) S. Ohnishi and H. M. McConnell, *J. Am. Chem. Soc.*, 1965, **87**, 2293; (b) W. L. Hubbell and H. M. McConnell, *Proc. Natl. Acad. Sci. USA*, 1969, **63**, 16–22; (c) W. L. Hubbell and H. M. McConnell, *Proc. Natl. Acad. Sci. USA*, 1969, **64**, 20–27; (d) R. D. Kornberg and H. M. McConnell, *Biochemistry*, 1971, **10**, 1111–1120; (e) P. Devaux and H. M. McConnell, *J. Am. Chem. Soc.*, 1972, **94**, 4475–4481; (f) *Spin Labeling*, ed. L. J. Berliner, Academic Press, New York, 1976; (g) *Spin Labeling II*, ed. L. J. Berliner, Academic Press, New York, 1976.
- L. J. Berliner, V. Khramtsov, H. Fujii and T. L. Clanton, *Free Radical Biol. Med.*, 2001, **5**, 489–499.
- (a) K. Yamada, I. Yamamiya and H. Utsumi, *Free Radical Biol. Med.*, 2006, **40**, 2040–2046; (b) H. Utsumi, K. Yasukawa, T. Soeda, K. Yamada, R. Shigemi, T. Yao and M. Tsuneyoshi, *J. Pharmacol. Exp. Ther.*, 2006, **317**, 228–235.
- (a) D. J. Lurie, D. M. Bussell and J. R. Mallard, *J. Magn. Reson.*, 1988, **76**, 366–370; (b) D. Grucker, T. Guiberteau, B. Eclancher, J. Chambron, R. Chiarelli, A. Rassat, G. Subra and B. Gallez, *J. Magn. Reson., Ser. B*, 1995, **106**, 101–109; (c) M. C. Krishna, S. English, K. Yamada, J. Yoo, R. Murugesan, N. Devasahayam, J. A. Cook, K. Golman, J. H. Ardenkjaer-Larsen, S. Subramanian and J. B. Mitchell, *Proc. Natl. Acad. Sci. USA*, 2002, **99**, 2216–2221; (d) D. J. Lurie, H. H. Li, S. Petryakov and S. J. L. Zweier, *Magn. Reson. Med.*, 2002, **47**, 181–186; (e) K. Golman, J. S. Petersson, J. H. Ardenkjaer-Larsen, I. Leunbach, L. G. Wistrand, G. Ehnholm and K. Liu, *J. Magn. Reson. Imaging*, 2002, **12**, 929–938; (f) S. Subramanian, K. Matsumoto, J. B. Mitchell and M. C. Krishna, *NMR Biomed.*, 2004, **17**, 263–294.
- (a) S. W. A. Blight, C. T. Harding, P. J. Sadler, R. A. Bulman, G. M. Bydder, J. M. Pennock, J. D. Kelly, I. A. Latham and J. A. Marriott, *Magn. Reson. Med.*, 1991, **17**, 516–532; (b) A. Mühler and O. Nalcioglu, *J. Magn. Reson. Imaging*, 1999, **9**, 177–186; (c) H. E. Daldrop-Link and R. C. Brasch, *Eur. Radiol.*, 2003, **13**, 354–365.
- B. D. Koivisto and R. G. Hicks, *Coord. Chem. Rev.*, 2005, **249**, 2612–2630.
- (a) R. Kuhn and H. Trischmann, *Monatsh. Chem.*, 1964, **95**, 457–479; (b) F. A. Neugebauer, H. Brunner and K. H. Hauser, *Tetrahedron*, 1971, **27**, 3623–3628; (c) K. Mukai, T. Yamamoto, M. Kohno, N. Azuma and K. Ishizu, *Bull. Chem. Soc. Jpn.*, 1974, **47**, 1797–1798.
- F. A. Neugebauer, H. Fisher and C. Krieger, *J. Chem. Soc., Perkin Trans. 2*, 1993, 535–544.
- (a) K. Mukai, in *Magnetic Properties of Organic Materials*, ed. P. M. Lahti, Marcel Dekker Inc., New York, 1999, ch. 21, pp. 427–447; (b) K. Mukai, in *Molecular Magnetism—New Magnetic Materials*, eds. K. Itoh and M. Kinoshita, Gordon and Breach Science Publishers, Netherlands, 2000, ch. 5.2, pp. 215–223.
- (a) K. Mukai, S. Kawasaki, J. B. Jamali and N. Achiwa, *Chem. Phys. Lett.*, 1995, **241**, 618–622; (b) M. Mito, H. Nakano, T. Kawae, M. Hitaka, S. Takaki, H. Deguchi, K. Suzuki, K. Mukai and K. Takeda, *J. Phys. Soc. Jpn.*, 1997, **66**, 2147–2156; (c) K. Mukai, M. Nuwa, K. Suzuki, S. Nagaoka, N. Achiwa and J. B. Jamali, *J. Phys. Chem. B*, 1998, **102**, 782–787; (d) M. Fujiwara, M. Tamura, M. Hara, K. Suzuki and K. Mukai, *J. Chem. Phys. B*, 2007, **111**, 9492–9495.
- G. F. Dvorko, E. A. Ponomareva and M. E. Ponomarev, *J. Phys. Org. Chem.*, 2004, **17**, 825–836.
- I. A. Bezvshenko and V. Kh. Premyslov, *Chem. Heterocycl. Compd.*, 1985, **21**, 946.
- A. J. Mayr, M. P. Eastman, C. J. Hartzell, D. Dong and C. McClellan, *J. Magn. Reson.*, 1992, **99**, 387–390.
- Y. Okahata and T. Kunitake, *J. Am. Chem. Soc.*, 1979, **101**, 5231–5234.
- G. M. Sheldick, *SHELX97-Programs for Crystal Structure Analysis (Release 97-2)*, 1998.
- B. Bleaney and K. D. Bowers, *Proc. R. Soc. London, Ser. A*, 1952, **214**, 451.
- J. M. Seddon, *Biochim. Biophys. Acta*, 1990, **1031**, 1–69.
- (a) G. Scheibe, *Angew. Chem.*, 1936, **49**, 563; (b) E. E. Jelly, *Nature*, 1936, **138**, 1009–1010.
- ESR measurements of PyC8TOV in lower concentrations than 0.5 mM is difficult due to the high dielectric constant of water, even using a capillary tube.
- E. M. Kosower, *An Introduction to Physical Organic Chemistry*, John Wiley & Sons, New York, 1968, ch. 2.6–2.8, pp. 293–342.
- The inverted absorption maxima ( $\lambda_{\max}^{-1}$ ) of acetonitrile–water solutions of PyC8TOV increased proportionally with the ratio of water. The intercept of  $\lambda_{\max}^{-1}$  was almost the same as of  $\lambda_{\max}^{-1}$  of an acetonitrile solution which was doubly distilled over CaH<sub>2</sub> (Fig. 9. point I).
- M. J. Plater, S. Kemp, E. Coronado, C. J. Gómez-García, R. W. Harrington and W. Clegg, *Polyhedron*, 2006, **25**, 2433.